Silicon (2018) 10:1861–1871
https://doi.org/10.1007/s12633-017-9690-2

ORIGINAL PAPER

Design and Properties of New Lead-Free Solder Joints Using Sn-3.5Ag-Cu Solder

Rizk Mostafa Shalaby[1] · Mustafa Kamal[1] · Esmail Abdo Mohammed Ali[2] · Mohammed S. Gumaan[1,2]

Received: 30 December 2015 / Accepted: 15 November 2017 / Published online: 11 April 2018

Abstract
This article aims to reduce the melting temperature of lead-free solder alloy and promote its mechanical properties. Eutectic tin-silver lead-free solder has a high melting temperature 221 °C used for electronic component soldering. This melting temperature, higher than that of lead–tin conventional eutectic solder, is about 183 °C. The effect of the melt spinning process and copper additions into eutectic Sn-Ag solder enhances the crystallite size to about 47.92 nm which leads to a decrease in the melting point to about 214.70 °C, where the reflow process for low heat-resistant components on print circuit boards needs lower melting point solder. The results showed the presence of intermetallic compound Ag_3Sn formed in nano-scale at the Sn-3.5Ag alloy due to short time solidification. The presence of new intermetallic compound, IMC from $Ag_{0.8}Sn_{0.2}$ and Ag phase improves the mechanical properties, and then enhances the micro-creep resistance especially at Sn-3.5Ag-0.7Cu. The higher Young's modulus of Sn-3.5Ag-0.5Cu alloy 55.356 GPa could be attributed to uniform distribution of eutectic phases. Disappearance of tin whiskers in most of the lead-free melt-spun alloys indicates reduction of the internal stresses. The stress exponent (n) values for all prepared alloys were from 4.6 to 5.9, this indicates to climb deformation mechanism. We recommend that the $Sn_{95.7}$-$Ag_{3.5}$-$Cu_{0.7}$ alloy has suitable mechanical properties, low internal friction 0.069, low pasty range 21.7 °C and low melting point 214.70 °C suitable for step soldering applications.

Keywords Lead-free solder · Melt-spun process · Microstructure · Mechanical properties · Melting behavior · Creep resistance

1 Introduction

The European parliament is taking steps to protect and improve the quality of the environment to protect human health and to use natural resources rationally and prudently, consequently nowadays Sn-Ag-Cu solders have been widely used in electronic industries as promising replacements for Sn-Pb solders [1]. There are some required features for the solders such as safety for human users, relatively low price, and low melting temperature, good wetting properties, low creep rate which result from high resistance to mechanical deformations and ability to be rapidly solidified. Tin has low cost, very good frictional properties due to its low friction and weak structure. So, when it is used in bearing solders applications, it is alloyed with some other metals [2]. The ternary Sn-Ag-Cu solder alloys have been selected as the first candidates due to their good joint properties, suitable melting points and good creep resistance which lead to high reliability [3–7]. McCormack et al. [8] have reported that the Sn–Ag alloys have moderate thermal resistance, high creep resistance and better ductility compared to Sn–Pb solder. The new lead-free and high Sn (about 96%) alloys may be susceptible to spontaneous growths of filament-like tin structures called tin whiskers [9]. The stress exponents for lead-free solders are relatively high values and are stable at temperatures ranging from 25 to 120 °C while those for Sn-37Pb decrease with increasing temperature. The stress exponent for Sn-37Pb at 120 °C (5.5) is very

✉ Rizk Mostafa Shalaby
rizk1969@mans.edu.eg; doctorrizk2@yahoo.co.uk
Mustafa Kamal
kamal42200274@yahoo.com
Mohammed S. Gumaan
m.gumaan1@gmail.com

[1] Metal Physics Laboratory, Physics Department, Faculty of Science, Mansoura University, Mansoura, Egypt

[2] Basic Science Department, Faculty of Engineering, University of Science and Technology, Sana'a, Yemen

close to that of pure Sn [6]. The lead-free solders have excellent creep resistance compared to the Sn–Pb eutectic solder where Ag_3Sn formation limits the strains and causes low creep rate [10]. Some alloying elements like Zn, Bi and In to Sn–3.5Ag eutectic alloy with high cooling rates enhance the IMCs formation, which thus increases the elastic moduli, hardness, strength and improves the mechanical performance, as well as lowering the melting temperature [11]. The importance of mechanical testing for solder joints comes from the necessity of momentum transport of the board to withstand the external shocks [12]. In microstructural properties, there are some factors

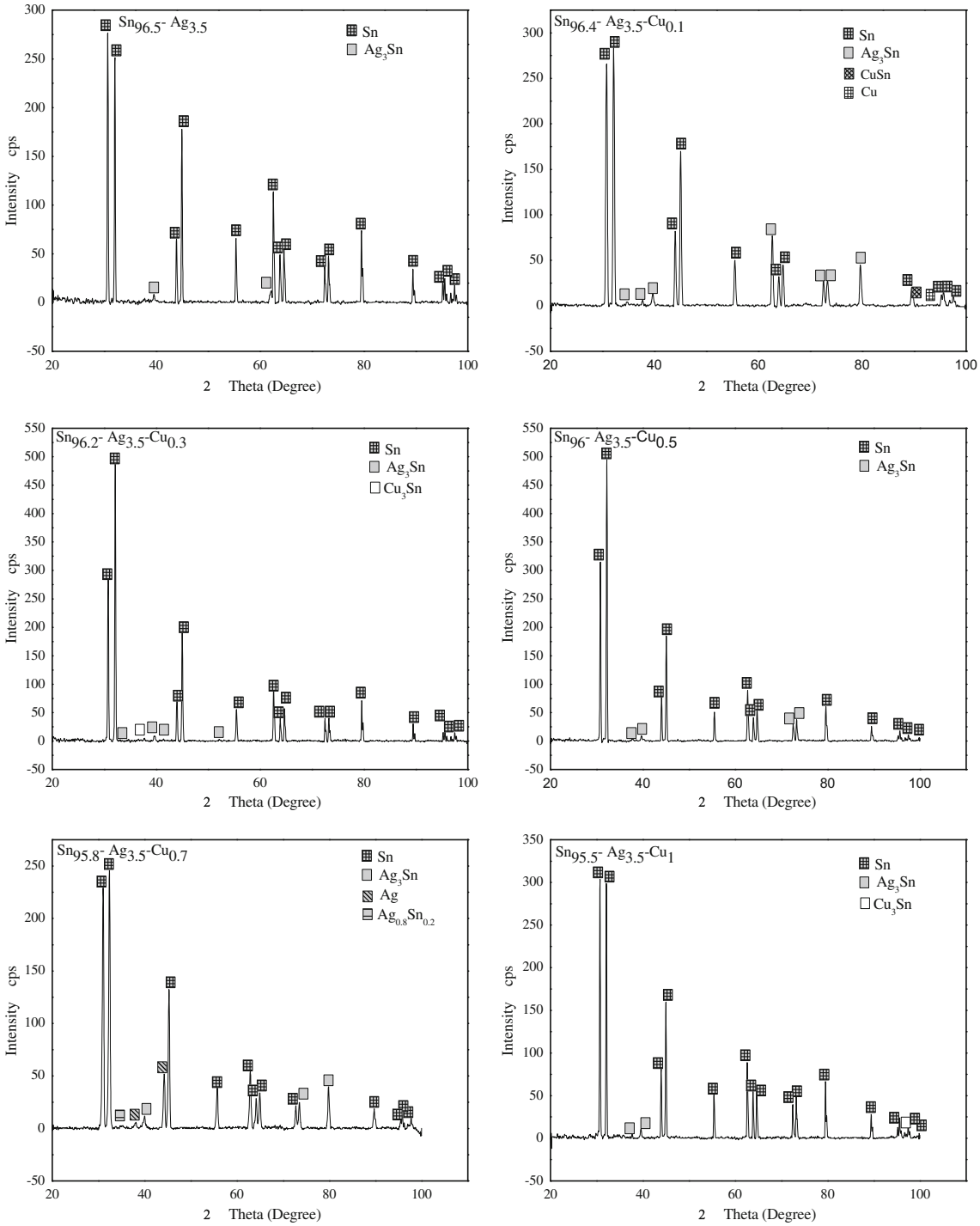

Fig. 1 X-ray diffraction patterns for solder alloys

that have potential effects such as presence of Ag_3Sn plates and ways to eliminate them, tin whiskers which cause electrical shorts also electro-migration failures in lead-free, flip-chip solder joints [13]. Some tin whiskers are nearly pure single crystals with excellent electrical conductivity [14]. Low creep rate showed in Sn-3.5Ag but when Cu content addition increased until 1.5 wt.%, the Cu_6Sn_5 coarsened and Ag_3Sn intermetallic was found, which led to high creep rate, thus there are determinates for alloying element concentrations [15]. The chemical method is successful in synthesis of lead-free systems with different Cu concentrations up to 1 wt.% doped to Sn-3.5Ag alloy nanoparticles which leads to reduction of their melting temperature to 215 °C [16]. Through reactions between Sn3.5Ag0.5Cu–0.5nano-TiO_2 and Cu substrate, scallop-type Cu_6Sn_5 grains formed at low temperature and changed to prism-type at high temperatures and vice versa at soldering time. It is also noted that the formed nano-Ag_3Sn intermetallic compound on the surface of Cu_6Sn_5 grains, decreases the surface energy and the growth of the Cu_6Sn_5 intermetallic compound is hindered [17]. This study aims to study properties, design and effect of low Cu concentrations on the eutectic Sn-3.5Ag bearing-solder melt-spun alloys.

2 Materials and Method

The lead-free solders were prepared from pure Sn, Ag and Cu (purity 99.99%) as raw materials. In order for material softening, refined and non-equilibrium crystallite sizes in material processing, elimination of micro-segregation right up to the amorphous state, the rapid solidification is required. This comes in an attempt to apply these benefits in the soldering process [18]. The chill-block melt-spinning is a widely used technique in material science due to its high cooling rates. It has been used in this work [19]. It is characterized by some advantages like low investment cost, high production speed, no environment pollution and a direct and simple process. The experimental utilized techniques have been described in detail in Kamal et al. [20], and are briefly will be described here. The solder alloys were prepared by melting the raw materials in an electric furnace and ejecting on a single roller method in air (melt spinning technique) with ≈2900 rpm with cooling rate about 3.7×10^5 K/sec [21]. They were prepared from Sn–3.5Ag–Cu_x (x = 0.0, 0.1, 0.3, 0.5, 0.7 and 1 by wt.%); melt-spun lead-free alloys. The value of solidification rate R is given by this formula: (R = t v/d), where v is the surface velocity of a roller, t is the sheet's thickness and d is the distance between the crucible nozzle and surface of a single roller which is approximately equal to 50 mm. After a part of one circle of a single roller the solid sheets will leave the surface roller with solidification rate R 10^{-5}–10^{-4} m/s. By using a sharp cutter, the melt-spun ribbons have suitable dimensions, width about 0.4 cm, thickness 0.063–0.095 mm. It is necessary to characterize the crystallography, and microstructure of the lead-free melt spun-ribbons using the x-ray diffraction technique and scanning electron microscopy (SEM). The dynamic resonance technique was used to identify the mechanical aspects for these alloys. The hardness and micro-creep resistance of ribbons were measured on a Vickers microhardness tester (Model FM7-Tech Group Tokoy-Japan) for dwell times up to 99 s. According to Juhasz [22] and Kamal [2], indentation creep was done by this model to calculate the stress exponent (n) in the steady-state creep by the following formula:

$$n = \left[\frac{\partial \ln \dot{d}}{\partial \ln H_V}\right]_d. \quad (1)$$

This equation is used to identify the deformation mechanisms, where the mechanism type will be identified from the stress exponent value, where H_V is the Vickers hardness number, d is the length of indentation diagonal, and $\dot{d}$ is the rate of variation in indentation diagonal length. A straight line would be obtained from plotting $\dot{d}$ against H_V on a double logarithmic scale, whose slope gives the stress exponent [23]. The x-ray diffraction analysis was implemented by CuKα radiation at room temperature [24]. Thermal properties were investigated by differential scanning calorimetry (DSC).

Table 1 Lattice and cell parameters for Sn–3.5Ag–Cu_x(x = 0.0, 0.1, 0.3, 0.5, 0.7 and 1 by wt.%) alloys

System in wt%	c/a of Sn-phase	Cell volume $(Å)^3$	Number of atoms per unit cell of tin phase
$Sn_{96.5}$-$Ag_{3.5}$	0.54588	108.1789	3.307
$Sn_{96.4}$-$Ag_{3.5}$-$Cu_{0.1}$	0.54879	108.0518	2.989
$Sn_{96.2}$-$Ag_{3.5}$-$Cu_{0.3}$	0.54745	107.9980	2.597
Sn_{96}-$Ag_{3.5}$-$Cu_{0.5}$	0.54751	107.8223	3.677
$Sn_{95.8}$-$Ag_{3.5}$-$Cu_{0.7}$	0.54013	107.7332	2.543
$Sn_{95.5}$-$Ag_{3.5}$-Cu_1	0.54580	108.0717	3.152

3 Results and Discussion of Significant Findings

3.1 Structural Characterizations

Duwez et al. [25] were the first researchers to have used the rapid cooling for metallic alloys. They obtained that the rapid solidification produces some benefits like increasing solid solubility and non-equilibrium phases or amorphous alloys. The patterns of X-ray diffraction obtained from the middle of the melt-spun ribbon for alloys are shown in Fig. 1. The $Sn_{96.5}$-$Ag_{3.5}$ alloy shown in Fig. 1a includes β-Sn phase with tetragonal structure, and Ag_3Sn intermetallic compound (IMC) phase with orthorhombic structure dispersed in the Sn-matrix. The $Sn_{96.4}$-$Ag_{3.5}$-$Cu_{0.1}$ alloy shown in Fig. 1b contains β-Sn phases and the number of peaks due to the Ag_3Sn intermetallic compound (IMC) phases and their intensities increased, since symmetry changing in cell volume is involved, and only one phase of Cu is in the Sn-matrix. Cu addition also enhances more Ag_3Sn intermetallic compounds formation. It is noticed that valance electron concentrations (VEC) and atomic size play a vital role in the formation of intermediate phase after rapid quenching from the melt [26]. The $Sn_{96.2}$-$Ag_{3.5}$-$Cu_{0.3}$ alloy shown in Fig. 1c contains β-Sn phase and Ag_3Sn intermetallic compound peaks, in addition to one phase of Cu_3Sn in the Sn-matrix. For the chemical reaction and its period of time taking place in IMC growth, Cu–Sn IMCs growth is believed to be diffusion-controlled [27]. Sn_{96}-$Ag_{3.5}$-$Cu_{0.5}$ alloy as shown in Fig. 1d contains β-Sn phases, and Ag_3Sn intermetallic compound phases dispersed in the Sn-matrix, and there is shifting for phases to the right side of the chart, also there are no other IMCs formed. For $Sn_{95.8}$-$Ag_{3.5}$-$Cu_{0.7}$ alloy shown in Fig. 1e, the alloy contains β-Sn, pure Ag phases, Ag_3Sn IMC and $Ag_{0.8}Sn_{0.2}$IMC. Finally, the $Sn_{95.5}$-$Ag_{3.5}$-Cu_1 alloy as shown in Fig. 1f contains β-Sn phase, and only two phases due to Ag_3Sn. Table 1 shows that the lowest values of axial ratio (c/a) and cell volume (V) were at 0.7 wt.% of Cu 0.540 and 107.733 respectively, this is due to increasing a-axis value where the c-axis is the stiffest [28]. Also, it shows that the cell volumes decrease with increasing Cu content and this may be because the atomic radius of Cu is smaller than the atomic radius of Sn. This value indicates to cell volume contraction (but still remains body centered tetragonal as β-Sn phase) at 0.7 wt.% of Cu addition which has near-complete solubility in Sn-matrix. In the equation $\sum A = \left(\frac{\rho V}{1.66020}\right) = n\,A$ [29], $\sum A$ is the sum of the atomic weight of atoms in the unit cell, ρ is the density (gm/cm^3), V is the volume of the unit cell (Å)^3, and n is the number of atoms per unit cell. The number of atoms per unit cell of Sn-phase must be an integer number (4 for β-Sn), but it is noted that the minimum value in the Table 1 is 2.543 at 0.7 wt.% Cu content; this points out to something missing (defects) in atoms resultant for fraction and it varies from cell to cell.

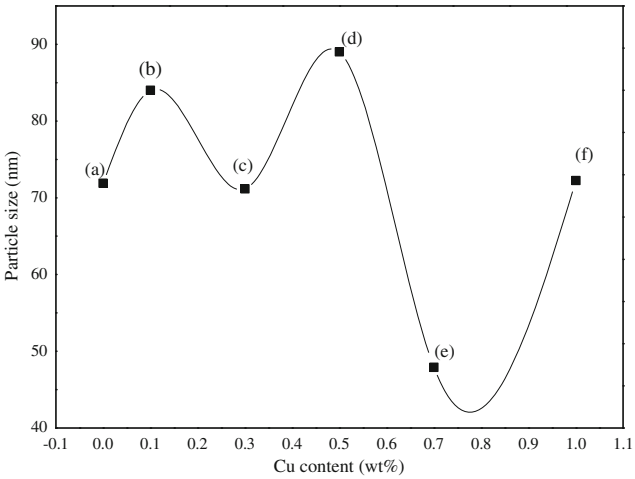

Fig. 2 Particle size versus Cu content for **a** $Sn_{96.5}$-$Ag_{3.5}$, **b** $Sn_{96.4}$-$Ag_{3.5}$-$Cu_{0.1}$, **c** $Sn_{96.1}$-$Ag_{3.5}$-$Cu_{0.3}$, **d** $Sn_{95.9}$-$Ag_{3.5}$-$Cu_{0.5}$, **e** $Sn_{95.7}$-$Ag_{3.5}$-$Cu_{0.7}$ and **f** $Sn_{95.5}$-$Ag_{3.5}$-Cu_1

3.2 Particle Size and Lattice Distortion

There is an inverse relationship between crystallite size and curve broadening; therefore, the size is estimated through the formula given by Scherrer's equation $t = (0.9\lambda/\mathrm{B}\cos\theta_B)$ [30], where B is the broadening of the diffraction line measured at half its maximum intensity (radians), t is the diameter of the crystal particle, θ_B is the Bragg angle and λ is the wavelength of x-rays. From Table 1 the non-integer number of atoms is used in this

Table 2 Particle size, lattice distortion and electron concentration (e/a) of crystalline phases for Sn–3.5Ag–Cu_x(x = 0.0, 0.1, 0.3, 0.5, 0.7 and 1 by wt.%) alloys

System in wt.%	Particle size(nm)	$1/D_{eff}\left(A^U\right)^{-1} \times 10^{-3}$	$5 < \varepsilon^2 > \frac{1}{2} \times 10^{-4}$	e/a
$Sn_{96.5}$-$Ag_{3.5}$	71.89	1.78	7.56	3.895
$Sn_{96.4}$-$Ag_{3.5}$-$Cu_{0.1}$	84.08	1.34	5.81	3.893
$Sn_{96.2}$-$Ag_{3.5}$-$Cu_{0.3}$	71.17	1.72	7.24	3.885
Sn_{96}-$Ag_{3.5}$-$Cu_{0.5}$	89.02	1.43	5.62	3.881
$Sn_{95.8}$-$Ag_{3.5}$-$Cu_{0.7}$	47.92	2.79	11.7	3.877
$Sn_{95.5}$-$Ag_{3.5}$-Cu_1	72.24	1.74	7.30	3.875

formula which is employed to calculate the crystallite size of small crystals using the full width half maximum (FWHM) of their diffraction curves. Past work [31] introduced two reasons for x-ray line broadening which could be either lattice distortions, or by lattice strain and small particles at the same time. In the x-ray diffracted lines there are perceivable changes in the intensity of lead-free solder peaks after rapid solidification using the spinning technique [19]. To derive information about the crystallite size (D_{eff}) and local lattice distortion (ε^2) in tin phases $B = \frac{1}{D_{eff}} + 5 < \varepsilon^2 >^{\frac{1}{2}} \frac{sin\theta}{\lambda}$ [32], the $\frac{1}{D_{eff}}$ and $5 < \varepsilon^2 >^{\frac{1}{2}}$ are given in Table 2. Figure 2 clarifies the particle size behavior with variation of Cu content from 0 to 1 wt.%. The lowest particle size is at 0.7 wt.% Cu content (alloy 5 in Table 2), these effects will be shown in most of the characteristics of the alloy. Lattice distortions for the tin-phase in all the lead-free melt-spun ribbons are very small as indicated in Table 2. This means approximately the best formation of the tetragonal system is close to the average electron number per atom (electron concentration) e/a = 4 as indicated in the Table 2, reflecting that the ordered pattern is dominant on the arrangement of atoms in the tin-phase. Such a crystal system has more stability than the random arrangement of atoms due to its lower energy and vice versa [33].

3.3 Microstructure

The microstructure of the ternary Sn-Ag-Cu melt-spun ribbons is shown in the SEM micrograph of Fig. 3e, f. Figure 3 shows the existence of a large number of grains having grain boundaries, black parts are Sn-matrix, and white areas are an eutectic structure which contains Ag_3Sn phase and β-Sn phase [34]. There is a fine dispersion throughout the microstructure and the formation of precipitator-free β-Sn dendrite globules has been

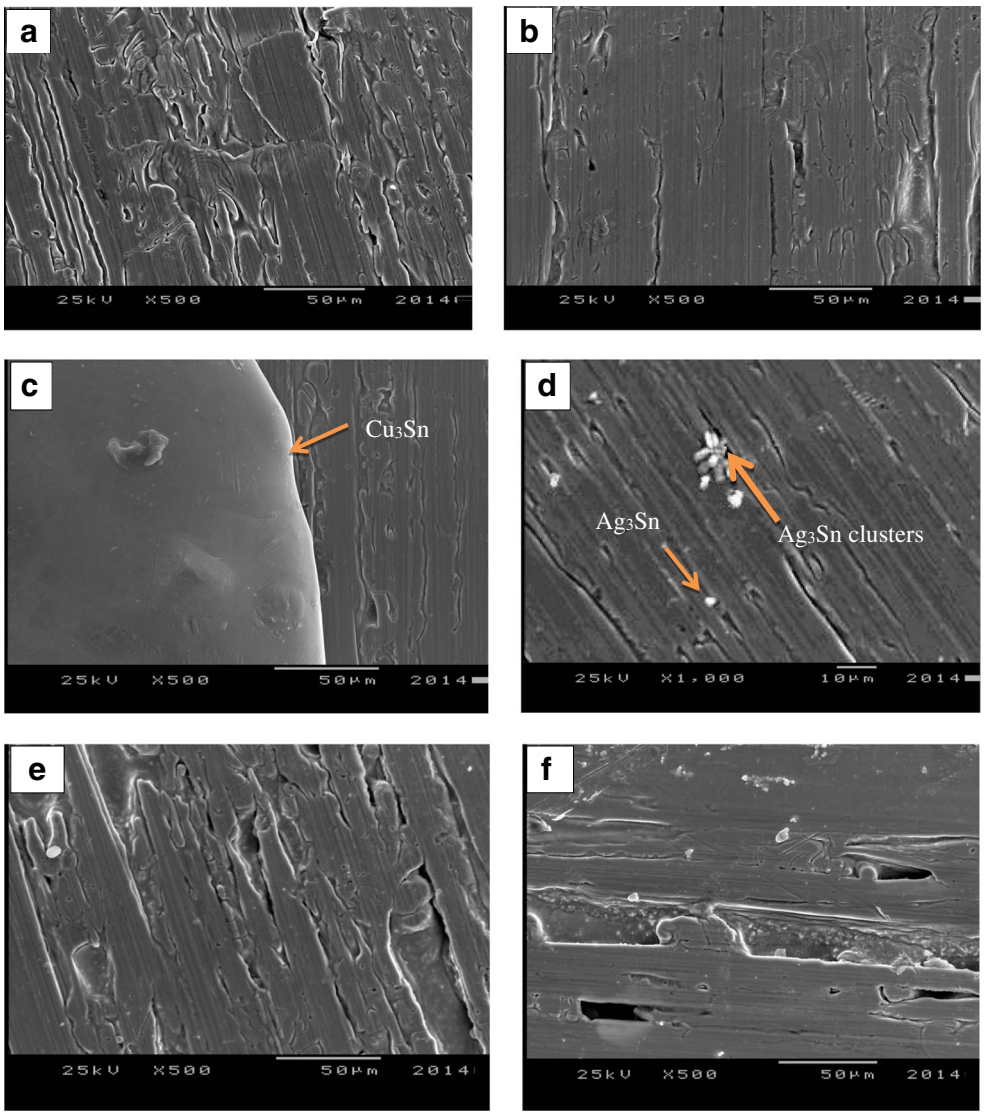

Fig. 3 SEM for **a** $Sn_{96.5}$-$Ag_{3.5}$, **b** $Sn_{96.4}$-$Ag_{3.5}$-$Cu_{0.1}$, **c** $Sn_{96.1}$-$Ag_{3.5}$-$Cu_{0.3}$, **d** $Sn_{95.9}$-$Ag_{3.5}$-$Cu_{0.5}$, **e** $Sn_{95.7}$-$Ag_{3.5}$-$Cu_{0.7}$ and **f** $Sn_{95.5}$-$Ag_{3.5}$-Cu_1

partially suppressed. However, in contrast to Fig. 3a, b, c and d possess smaller, more irregularly shaped eutectic colonies. Moreover Fig. 3a, b reveal tin whiskers which grow due to internal stresses. Whisker growth is not affected more in solder properties but long whiskers may cause short circuits in printed circuit assemblies [35]. It has been observed that the addition of small amounts of Cu at the level of 0.7% in the Sn-Ag binary eutectic solder reduces

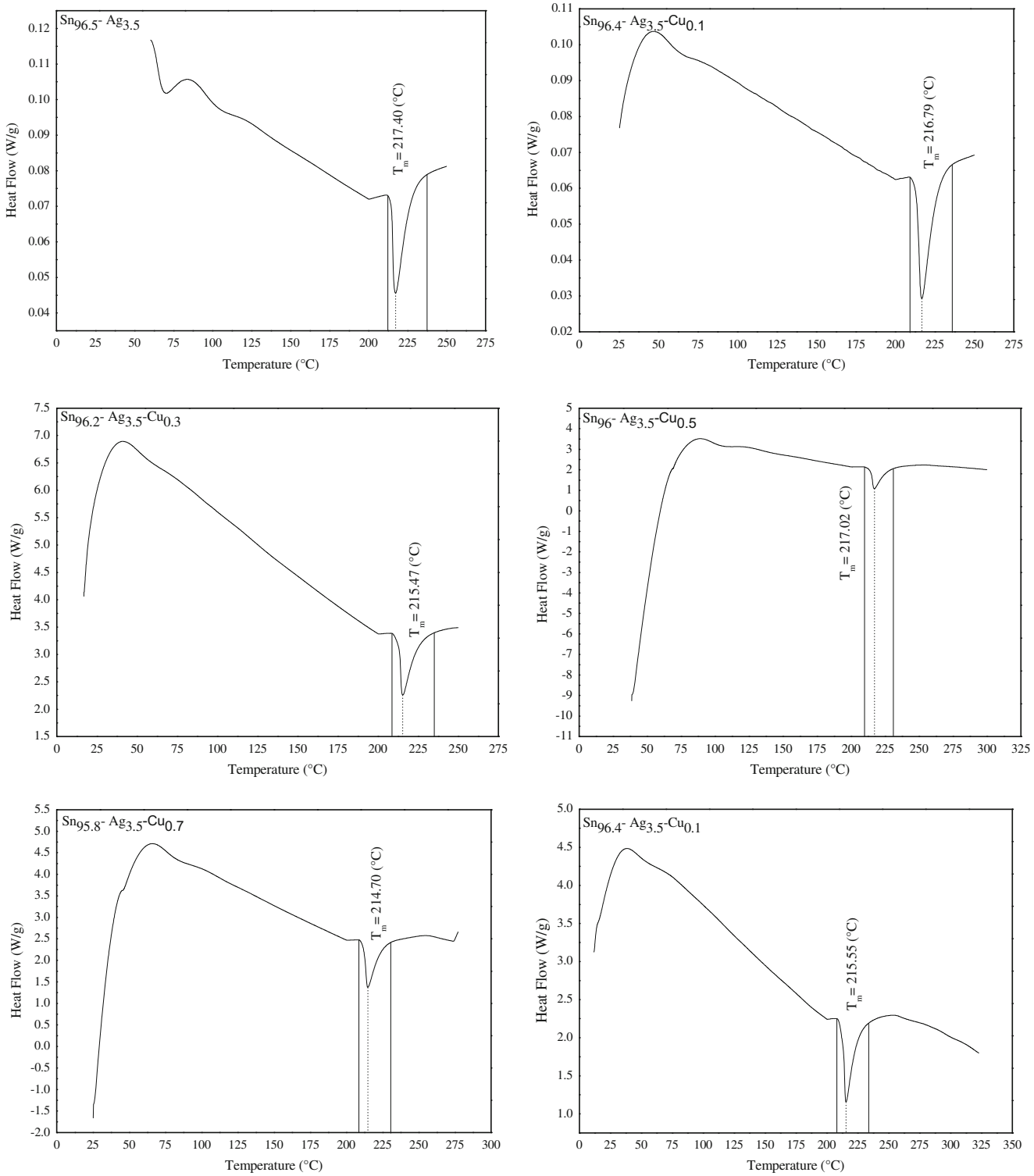

Fig. 4 Differential scanning calorimetry (DSC) melting curves for solder alloys

the effective grain size and retains the fine dispersion of Ag-rich precipitates in the β-Sn matrix throughout the solidification microstructure. Figure 3a shows nano-Ag_3Sn particles which formed and precipitated on the Sn-matrix confirming with Tsao [17], and this is ascribed to the high cooling rate of the melt-spinning technique. In Fig. 3d, the nano-Ag_3Sn IMC precipitates on the vacancies and tends to be segregated clusters; they are also located on these vacancies and grain boundaries. Therefore, it increases the resistance to dislocation and improves the mechanical properties and creep behavior.

3.4 Thermal Properties

Melting temperature is a vital thermal property where a solder alloy should have a low melting temperature zone [36]. Figure 4 shows the DSC endothermic peaks of Sn–3.5Ag–Cu_x(x = %(0.0, 0.1, 0.3, 0.5, 0.7 and 1)) melt-spun lead-free alloys during heating. The melting behavior for each of them was investigated by differential scanning calorimetry (DSC) in an argon atmosphere at a heating rate of 10 °C/min. For $Sn_{96.5}$-$Ag_{3.5}$ alloy, the melting point is equal to 217.4 °C which decreases approximately by 4 °C than that obtained by normal techniques. The melt-spinning technique has the effect to remove the alloys from the equilibrium state and therefore decreases the melting temperature. Also, in $Sn_{96.5}$-$Ag_{3.5}$ and $Sn_{96.4}$-$Ag_{3.5}$-$Cu_{0.1}$ alloys, there are two endothermic peaks indicating rearrangement of the metastable phases. After that, there are effects of Cu additions to the Sn–3.5Ag alloy as follows: Sn–3.5Ag–Cu_x(x = %(0.1, 0.3, 0.5, 0.7 and 1)) melt-spun lead-free alloys, Cu additions have changed melting point except at %.0.5 Cu. Zu et al. [37] stated that in the molten alloys the structural changes slightly rise as a function of temperature, this fact proved by the corresponding endothermic peak in a differential scanning calorimeter. So, the reducing of melting point at 0.7wt.% of Cu is related to particle size of β-Sn, where the hard inclusions (Cu atoms) cause β-Sn to stop growing [38]. Increasing particle size at 0.5 wt.% Cu may refer to insufficient Cu atoms which should suppress β-Sn growth. Table 3 shows the melting point (T_m), solidus temperature (T_s), liquidus temperature (T_l), enthalpy of fusion (ΔH_f), specific heat C_p, entropy change and pasty range of these alloys which are calculated and resulted from Fig. 4. Among ternary alloys the $Sn_{95.8}$-$Ag_{3.5}$-$Cu_{0.7}$ has the lowest pasty range value, where this is preferable for the soldering process.

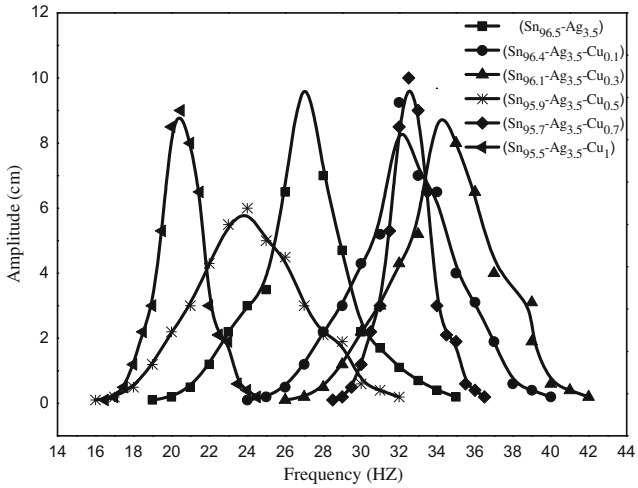

Fig. 5 Resonance curves for **a** $Sn_{96.5}$-$Ag_{3.5}$, **b** $Sn_{96.4}$-$Ag_{3.5}$-$Cu_{0.1}$, **c** $Sn_{96.1}$-$Ag_{3.5}$-$Cu_{0.3}$, **d** $Sn_{95.9}$-$Ag_{3.5}$-$Cu_{0.5}$, **e** $Sn_{95.7}$-$Ag_{3.5}$-$Cu_{0.7}$ and **f** $Sn_{95.5}$-$Ag_{3.5}$-Cu_1

3.5 Mechanical Properties

3.5.1 Internal Friction and Dynamic Young's Modulus

Figure 5 shows the curves resulting from the dynamic resonance technique for Sn–3.5Ag–Cu_x(x = 0.0, 0.1, 0.3, 0.5, 0.7 and 1 wt.%) alloys.

Table 4 shows the internal friction against Young's modulus for prepared alloys. Dynamic techniques are preferable methods for the determination of Young's modulus for solders; Young's modulus is slightly affected by alloying additions [39]. It is concluded that the internal friction is responsive to Cu content in Sn–3.5Ag–Cu_x(x = %(0.0, 0.1, 0.3, 0.5, 0.7 and 1) lead-free alloys as indicated in Table 4. Internal friction and Young's

Table 3 The melting point (T_m), solidus temperature (T_s), liquidus temperature (T_l), enthalpy of fusion (ΔH_f), specific heat C_p, entropy change and pasty range for Sn–3.5Ag–Cu_x(x = 0.0, 0.1, 0.3, 0.5, 0.7 and 1 by wt.%) alloys

System in wt%	T_l(°C)	T_m(°C)	T_s (°C)	Enthalpy ΔH (j/g)	Specific heat C_p(j/g.k)	Entropy change S (j/g.k)	Pastry range (°C)
$Sn_{96.5}$-$Ag_{3.5}$	217.40	217.40	217.40	1.391	0.067	2.80	0
$Sn_{96.4}$-$Ag_{3.5}$-$Cu_{0.1}$	236.5	216.79	209.25	1.842	0.070	3.72	27.7
$Sn_{96.2}$-$Ag_{3.5}$-$Cu_{0.3}$	235	215.47	208.04	56.8	1.893	114.53	26.9
Sn_{96}-$Ag_{3.5}$-$Cu_{0.5}$	231	217.02	209.87	50.82	2.258	102.31	21.13
$Sn_{95.8}$-$Ag_{3.5}$-$Cu_{0.7}$	231	214.70	209.30	49.28	2.24	99.76	21.7
$Sn_{95.5}$-$Ag_{3.5}$-Cu_1	234	215.55	208.46	56.41	2.169	114.08	25.54

Table 4 Internal friction (Q^{-1}) values and Young's modulus for Sn–3.5Ag–Cu_x(x = 0.0, 0.1, 0.3, 0.5, 0.7 and 1 by wt.%) alloys

System in wt%	$Q^{-1} \times 10^{-3}$	E (GPa)
$Sn_{96.5}$-$Ag_{3.5}$	98.2	35.031
$Sn_{96.4}$-$Ag_{3.5}$-$Cu_{0.1}$	91.6	36.988
$Sn_{96.2}$-$Ag_{3.5}$-$Cu_{0.3}$	72.4	37.499
Sn_{96}-$Ag_{3.5}$-$Cu_{0.5}$	65.4	55.356
$Sn_{95.8}$-$Ag_{3.5}$-$Cu_{0.7}$	69.6	31.219
$Sn_{95.5}$-$Ag_{3.5}$-Cu_1	106.9	29.876

modulus values for Sn-3.5%Ag alloy are 0.0982, and 35.031 MPa respectively. Theoretically, Young's modulus (E) for Sn-3.5%Ag should be above 50 MPa. Dropping E values are attributed to agglomeration and segregation of nano-Ag_3Sn particles to become accumulated over each other, so these results are in agreement with Sun et al. [40]. After copper additions from 0.1 to 0.5 wt.% to the eutectic Sn-3.5%Ag alloy, it is noticed that there is decreasing internal friction (Q^{-1}) with increasing Young's modulus (E). There is also a substantial drop in (E) values with substantial increase in (Q^{-1}) which may refer to intermetallic compounds sliding over the Sn-matrix. This conduct of Young's modulus (E) can clarify the change in c/a ratio of the unit cell of β-Sn. This may be attributed to an increased value of c/a ratio which means expanding the unit cell of β-Sn. Theoretically, with extension of the unit cell, the alloy becomes weak but experimentally Young's modulus (E) increases; it is due to the presence of intermetallic compounds whose inclusions in the Sn-matrix caused more resistance for deformations. High elastic modulus (E) of any material can be desirable or undesirable depending on the required performance attribute. So, at high strain rate applications, higher modulus of bulk solders results in lower life time [41–43]. Consequently, the $Sn_{95.8}$-$Ag_{3.5}$-$Cu_{0.7}$ melt-spun alloy is suitable for high strain rate applications.

3.5.2 Hardness Indentation and Micro-Creep Behavior

A standard load is pressed on the surface area by a hard indenter, as illustrated in Fig. 6 which shows the variation of the strain (ΔS/S) with time (s) at constant load equal to 0.098 N by using Hv = 0.102 F/S (MPa), where F is the test load (N), and S is the surface area of an indentation (mm^2). Here the strain is considered a change in area given by; (ΔS/S)%, where $S = S - S_o$ and S_o is considered to be the area at the minimum indentation time [36, 37]. In this curve, it is noted that the melt-spun alloys $Sn_{96.4}$-$Ag_{3.5}$, $Sn_{96.2}$-$Ag_{3.5}$-$Cu_{0.3}$, and $Sn_{95.8}$-$Ag_{3.5}$-$Cu_{0.7}$ have less strain and stay more stable with increasing time at constant load; this may be attributed to the refinement of grain size which leads to more grain boundaries. Since grain boundaries sometimes

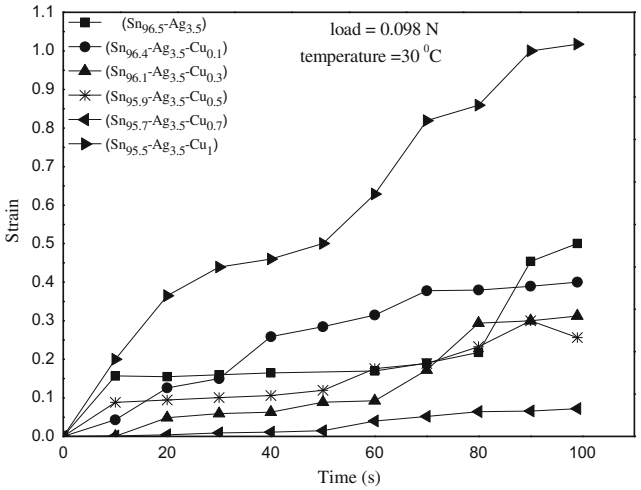

Fig. 6 Variation of strain (ΔS/S) with dwell time (s)

act as obstructions of dislocations and hinder their motion, Sn_{96}-$Ag_{3.5}$-$Cu_{0.5}$ melt-spun alloys have dropped in strain in the last interval of time. This gives it more importance to resist loads in bearing solder applications. As $Sn_{96.4}$-$Ag_{3.5}$-$Cu_{0.1}$ and $Sn_{95.5}$-$Ag_{3.5}$-Cu_1 melt-spun alloys appear to show more strain, the maximum strain for the $Sn_{95.5}$-$Ag_{3.5}$-Cu_1 melt-spun alloy may be due to lattice distortion of this alloy which is relatively higher than other alloys as shown in Table 2. Due to work hardening in three creep stages (primary, secondary and tertiary) the strain rate is relatively high in the primary stage and becomes near constant at the secondary or steady state stage due to strain hardening balanced with softening (removal of dislocations), fracture always occurs at the tertiary stage but our curve only reaches to the first and second stages [44]. Figure 7 shows variation of Vickers microhardness H_v with time. From this curve, it is noted that the hardness of melt-spun alloys at the starting point 5 s is as follows:

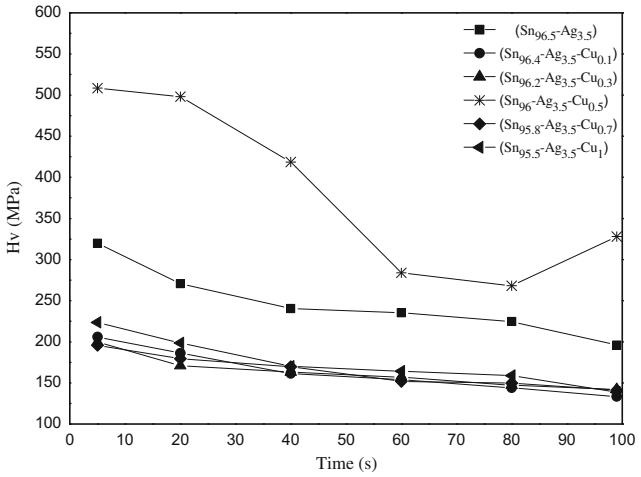

Fig. 7 Variation of microhardness H_v (MPa) with dwell time (s)

H_v gradually increases with increasing Cu content up to %wt.0.5 Cu, then H_v decreases with increasing Cu content. This is exactly identical with structural analysis, Young's modulus (E) and internal friction (Q^{-1}). Figure 7 shows the variation (decreases) of $H_v$with time for all alloys at constant load (0.098N), but the Sn-3.5%Ag-0.5%Cu alloy has increased in H_v at the last time interval, after that the $Sn_{95.8}$-$Ag_{3.5}$-$Cu_{0.7}$ alloy has high H_v and is more stabilized.

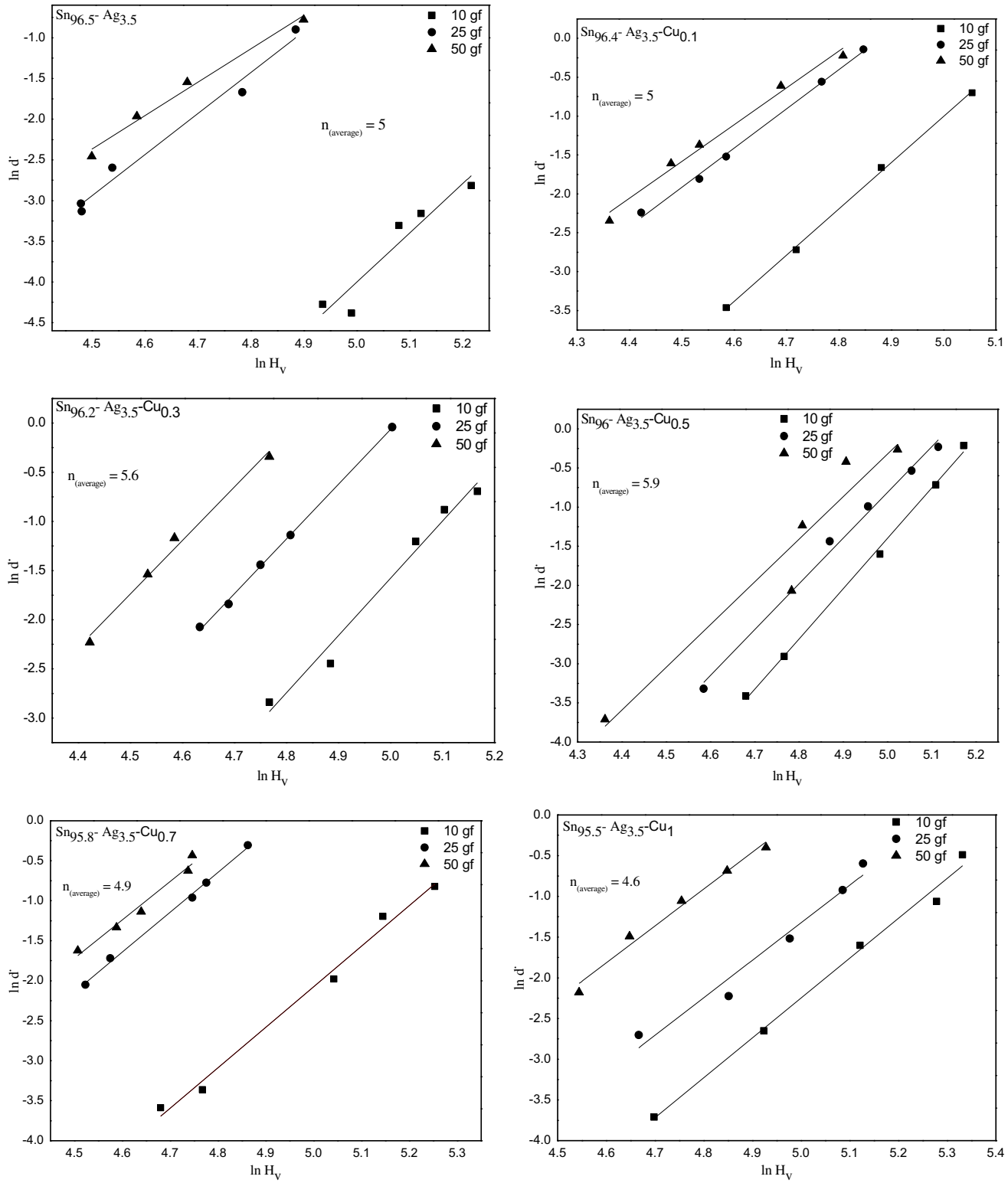

Fig. 8 Ln–Ln plot of the rate of diagonal variation against the Vickers hardness numbers for solder alloys

Table 5 The stress exponent values (n) for Sn–3.5Ag–Cu_x (x = 0.0, 0.1, 0.3, 0.5, 0.7 and 1 by wt.%) alloys

System wt%	Stress exponent (n_{ave})
$Sn_{96.5}$-$Ag_{3.5}$	5.0
$Sn_{96.4}$-$Ag_{3.5}$-$Cu_{0.1}$	5.2
$Sn_{96.2}$-$Ag_{3.5}$-$Cu_{0.3}$	5.6
Sn_{96}-$Ag_{3.5}$-$Cu_{0.5}$	5.9
$Sn_{95.8}$-$Ag_{3.5}$-$Cu_{0.7}$	4.9
$Sn_{95.5}$-$Ag_{3.5}$-Cu_{1}	4.6

It was selected as one of the three methods to dissect and to calculate the stress exponent of indentation creep (n) of Mahmudi et al. [23], and to measure the stress exponent of these alloys at room temperature [2]. By using Eq. 1 the straight line resulting from ˙d plotted against H_v on double logarithmic scale, and the slope of the straight line gives the stress exponent (n). From Fig. 8, the average slope (n) resulting from the straight lines is obtained for each lead-free melt-spun alloy at 10, 25 and 50 gram force loads. The stress exponent values obtained from the experimental method are shown in Table 5. The previous studies enhance using of the deformation mechanism map to determine the type of preponderant creep mechanism according to the stress exponent values. However, the stress exponent gave us an indication of the climb deformation mechanism during room temperature. The ternary Sn_{96}-$Ag_{3.5}$-$Cu_{0.5}$ and $Sn_{95.8}$-$Ag_{3.5}$-$Cu_{0.7}$ alloys have higher (n) value (5.9), which means high resistance to creep deformation to other alloys which are basically more agreeable to the structural and mechanical analysis; the above n value is approximately equal to the result obtained in [45]. The small difference between the results is due to the difference in work done temperatures. Reduced n values for other lead-free solders may be due to the nucleation and growth of voids at IMCs on grain boundaries because of the incompatibility of creep flow between the Sn-matrix and the IMC [45, 46].

4 Conclusions

The structural, mechanical, thermal and microstructural properties of the Sn-Ag based low melting point solders, especially the Sn-Ag-Cu solder family, were studied by means of XRD, H_V, DRT, DSC and SEM. The results are as follows:

1 Disappearance of tin whiskers in most lead-free melt-spun alloys indicates the lack of internal stresses.
2 Cu addition enhances the Ag_3Sn IMCs formation and increases their sizes, Cu additions as Cu_X (X = %(0.1, 0.3, 0.5, 0.7 and 1)) to Sn–3.5Ag melt-spun lead-free alloy cause improvement in mechanical properties, and delay the fracture and creep resistance.
3 Sn_{96}-$Ag_{3.5}$-$Cu_{0.5}$ and $Sn_{95.8}$-$Ag_{3.5}$-$Cu_{0.7}$ have an order state and uniform distribution of eutectic phases, so they have approximately better structural, thermal, mechanical properties and high resistance to creep deformation at room temperature due to additional IMCs formation, thus are suitable for bearing solders applications.
4 The stress exponent in these alloys indicates the climb deformation mechanism during room temperature.
5 The joint reliability of the Sn-Ag-Cu solder is comparable to that of Sn-Pb eutectic solder, thereby making this solder a potential candidate for extension of the lead-free circuit manufacturing process.

References

1. Liew MC, Ahmad I, Lee LM et al (2012) Corrosion behavior of Sn-3.0Ag-0.5Cu lead-free solder in potassium hydroxide electrolyte. Metall Mater Trans A Phys Metall Mater Sci 43:3742–3747
2. Kamal M, El-Bediwi A, Lashin AR, El-Zarka AH (2011) Copper effects in mechanical properties of rapidly solidified Sn-Pb-Sb Babbitt bearing alloys. Mater Sci Eng A 530:327–332
3. Rosalbino F, Angelini E, Zanicchi G, Marazza R (2008) Corrosion behaviour assessment of lead-free Sn-Ag-M (M = In, Bi, Cu) solder alloys. Mater Chem Phys 109:386–391
4. Zhang XP, Yu CB, Zhang YP et al (2007) Processing treatment of a lead-free Sn-Ag-Cu-Bi solder by rapid laser-beam reflowing and the creep property of its soldered connection. J Mater Process Technol 192–193:539–542
5. Suh D, Kim D, Liu P, Kim H (2007) Effects of Ag content on fracture resistance of Sn–Ag–Cu lead-free solders under high-strain rate conditions. Mater Sci Eng A 460:595–603
6. Shohji I, Yoshida T, Takahashi T, Hioki S (2004) Tensile properties of Sn–Ag based lead-free solders and strain rate sensitivity. Mater Sci Eng A 366:50–55
7. Sun L, Chen M, Zhang L, Yang F (2017) Microstructures evolution and properties of Sn-Ag-Cu solder joints. Acta Metall Sin 53:615–621
8. Mccormack M, Jin S (1994) Improved mechanical properties in new, Pb-free solder alloys. J Electron Mater 23:715–720
9. Meschter S, Snugovsky P, Bagheri Z et al (2014) Whisker formation on SAC305 soldered assemblies. JOM 66:2320–2333
10. Shohji I, Yasuda K, Takemoto T (2005) Estimation of thermal fatigue resistances of Sn-Ag and Sn-Ag-Cu lead-free solders using strain rate sensitivity index. Mater Trans 46(11):2329-2334
11. Shalaby RM (2010) Effect of rapid solidification on mechanical properties of a lead free Sn-3.5Ag solder. J Alloys Compd 505:113–117
12. Williamson DM, Field JE, Palmer SJP, Siviour CR (2007) Rate dependent strengths of some solder joints. J Phys D Appl Phys 40:4691–4700
13. Puttlitz KJ, Galyon GT (2007) Impact of the ROHS directive on high-performance electronic systems Part I: need for lead utilization in exempt systems. Lead-Free Electron Solder A Spec Issue J Mater Sci Mater Electron 40:331–346
14. Galyon GT (2005) Annotated tin whisker bibliography and anthology. IEEE Trans Electron Packag Manuf 28:94–122

15. Shin SW, Yu J (2005) Creep deformation of Sn-3.5Ag-xCu and Sn-3.5Ag-xBi solder joints. J Electron Mater 34:188–195
16. Pan HJ (2011) Synthesis of Sn-3.5Ag alloy nanosolder by chemical reduction method. Mater Sci Appl 2:1480–1484
17. Tsao LC (2011) Evolution of nano-Ag3Sn particle formation on Cu-Sn intermetallic compounds of Sn3.5Ag0.5Cu composite solder/Cu during soldering. J Alloys Compd 509:2326–2333
18. Rosen G, Avissar J, Gefen Y, Baram J (1987) Centrifuge melt spinning. J Phys E 20:571–574
19. Kamal M, Mohammad U (2012) A review: chill-block melt spin technique, theories & applications ISBN: 978-1-60805-151-9, Bentham e Books, Bentham Science Publishers
20. Kamal M, Gouda E (2008) Effect of zinc additions on structure and properties of Sn–Ag eutectic lead-free solder alloy. J Mater Sci Mater Electron 19:81–84
21. El-Bediwi A, Lashin AR, Mossa M, Kamal M (2011) Indentation creep and mechanical properties of quaternary Sn-Sb based alloys. Mater Sci Eng A 528:3568–3572
22. Juhász A, Tasnádi P, Kovács I (1986) Superplastic indentation creep of lead—tin eutectic. J Mater Sci Lett 5:35–36
23. Roumina R, Raeisinia B, Mahmudi R (2004) Room temperature indentation creep of cast Pb-Sb alloys. Scr Mater 51:497–502
24. Kamal M, El-Bediwi A, Jomaan M (2012) Rapid quenching of liquid lead base alloys for high performance storage battery applications, IJET-IJENS, 12, 06
25. Duwez P, Willens RH, Klement W (1960) Metastable electron compound in Ag-Ge alloys. J Appl Phys 31:1137
26. Giessen BC, Grant NJ (1965) New intermediate phases in transition metal systems, III. Acta Crystallogr 18:1080–1081
27. Li JF, Agyakwa PA, Johnson CM (2012) Effect of trace Al on growth rates of intermetallic compound layers between Sn-based solders and Cu substrate. J Alloys Compd 545:70–79
28. Bieler TR, Jiang H (2006) Influence of Sn grain size and orientation on the thermomechanical response and reliability of Pb-free solder joints. IEEE Trans Compon Packag Technol 31(2):1462–1467
29. Cullity BD (1959) Elements of X-ray diffraction, vol 262. Addison-Wesley Publishing Company, USA, p 317
30. Kamal M, El-Bediwi A-B, Shalaby R, Younus M (2015) A study of eutectic indium-bismuth and indium-bismuth-tin Field's metal rapidly solidified from melt. J Adv Phys 7:1404–1413
31. Van Arkel EA (1925) Über die Verformung des Kristallgitters von Metallen durch mechanische Bearbeitung. Physica 34:208–212
32. Williamson G, Hall W (1953) X-ray line broadening from filed aluminium and wolfram. Acta Metall 1:22–31
33. Kamal M, El-Bediwi A-B (2000) Structure, mechanical metallurgy and electrical transport properties of rapidly solidified $Pb_{50}Sn_{50-x}Bi_x$ alloys. J Mater Sci Mater Electron 11(6):519–523
34. Shimoda M, Hidaka N, Watanabe H, Yoshiba M (2011) High temperature creep properties of Sn-3.5 Ag and Sn-5Sb lead-free solder alloys. Trans JWRI 40:2
35. Kumar R (2014) Effect of Ag on Sn-Cu lead free solders effect of Ag on Sn-Cu lead free solders. Thesis of PhD in Department of Metallurgical and Materials Engineering National Institute Of Technology, Rourkela
36. Shalaby RM (2013) Effect of silver and indium addition on mechanical properties and indentation creep behavior of rapidly solidified Bi-Sn based lead-free solder alloys. Mater Sci Eng A 560:86–95
37. Zu FQ, Zhu ZG, Zhang B et al (2001) Post-melting anomaly of Pb-Bi alloys observed by internal friction technique. J Phys Condens Matter 13:11435–11442
38. Sweatman K, Mcdonald SD, Whitewick M et al (2013) Grain refinement for improved lead-free solder joint reliability. In: Proceedings of IPC APEX EXPO Conference & Exhibition 2013, APEX EXPO 2013, San Diego, United States, pp 561-589
39. Yi-Wen C, Thomas AS (2003) Predicting tensile properties of the bulk 96.5Sn-3.5Ag lead-free solder. J Electron Mater (32) 6(2003):1–19
40. Sun L, Zhang L (2015) Properties and microstructures of Sn-Ag-Cu-X lead-free solder. Adv Mater Sci Eng 2015:1–16
41. Pandher RS, Lewis BG, Vangaveti R, Singh B (2007) Drop shock reliability of lead-free alloys—effect of micro-additives. In: Proceedings - electronic components and technology conference, pp 669–676
42. El-Ashram T, Shalaby RM (2005) Effect of rapid solidification and small additions of Zn and Bi on the structure and properties of Sn-Cu eutectic alloy. J Electron Mater 34:212–215
43. Kamal M, El-Ashram T (2007) Microcreep of rapidly solidified Sn–0.7 wt.% Cu–In solder alloys. Mater Sci Eng A 456:1–4
44. Shalaby RM (2015) Indium, chromium and nickel-modified eutectic Sn–0.7 wt% Cu lead-free solder rapidly solidified from molten state. J Mater Sci Mater Electron 26:6625–6632
45. Lin C, Chu D (2005) Creep rupture of lead-free Sn-3. 5Ag and Sn-3. 5Ag-0. 5Cu solders. J Mater Sci Mater Electron 16:355–365
46. Gumaan MS, Ali EA, Shalaby RM, Kamal M (2016) Improvement of the mechanical properties of Sn-Ag-Sb lead-free solders: effects of Sb addition and rapidly solidified. PCIM Eur 2016; Int Exhib Conf Power Electron Intell Motion, Renew Energy Energy Manag 9